C. R. Physique 14 (2013) 564–577

Contents lists available at SciVerse ScienceDirect

Comptes Rendus Physique

www.sciencedirect.com

Trends and perspectives in solid-state wetting / Mouillage solide–solide : tendances et perspectives

A model for solid-state dewetting of a fully-faceted thin film

Un modèle pour le démouillage solide–solide d'un film mince complètement facetté

Rachel V. Zucker *, Gye Hyun Kim, W. Craig Carter, Carl V. Thompson

Department of Materials Science and Engineering, Massachusetts Institute of Technology, Cambridge, MA, USA

ARTICLE INFO

Article history:
Available online 12 August 2013

Keywords:
Thin films
Dewetting
Capillarity
Crystalline
Anisotropic
Solid-state

Mots-clés :
Films minces
Démouillage
Capillarité
Milieux crystallins
Anisotropie
État solide

ABSTRACT

Owing to their extremely aspect ratios, most thin films are unstable and when they are heated, they will dewet or agglomerate to form islands. This process can occur in the solid state through capillary-driven surface self-diffusion. A key feature of the dewetting process is the retraction of the edges of the film, either natural edges, patterned edges, or edges where holes have formed. Models of edge retraction have been previously developed for isotropic materials and anisotropic materials with differentiable surfaces, but the effects of faceting in highly anisotropic materials have been largely unexplored. Here, we present a two-dimensional model of edge retraction for highly anisotropic, fully-faceted thin films. This model shows generally good agreement with experimental results for edge retraction of single-crystal Ni films on MgO. In both experiments and the model, rims form as the edges retract. The effects of adjusting various physical parameters on the edge retraction rate and the evolving rim geometry were explored using the model. The film thickness, surface self-diffusivity on the top facet of the rim, the equivalent contact angle of the film on the substrate, and the absolute value of the surface energies were found to be the factors that have the greatest influence on the edge retraction rate. In isotropic models and some experimental systems, valleys form ahead of the retracting rims and deepen to contact the substrate and cause pinch-off. Our model suggests that this form of pinch-off will not occur when the rim is fully faceted and the top surface is an equilibrium facet. However, pinch-off can occur through film thinning and for films with top surfaces that do not form flat equilibrium facets.

RÉSUMÉ

Du fait de leurs rapports d'aspect extrêmement élevés, la plupart des films fins sont instables et, lorsqu'ils sont chauffés, ils démouillent ou s'agglomèrent pour former des îlots. Ce processus peut se produire à l'état solide grâce à la diffusion de surface induite par la capillarité. Un trait caractéristique du processus de démouillage est la rétractation des bords du film, qu'ils soient naturels ou structurés, ou autour des trous qui se forment dans le film. Des modèles de rétractation de bords ont été précédemment développés pour des matériaux isotropes et anisotropes avec des surfaces différentiables, mais les effets du facettage dans les matériaux hautement anisotropes sont largement inexplorés. Nous présentons ici un modèle à deux dimensions de la rétractation des bords pour des films minces hautement anisotropes, complètement facettés. Ce modèle montre généralement un bon accord avec les résultats expérimentaux pour la rétractation de films de nickel monocristallins sur MgO. À la fois dans les expériences et le modèle, des fronts se forment lorsque les bords se rétractent. Les effets de l'ajustement de divers paramètres physiques sur le taux de rétractation des bords et la géométrie des bourrelets en évolution

1631-0705/$ – see front matter
http://dx.doi.org/10.1016/j.crhy.2013.06.005

ont été explorés en utilisant le modèle. L'épaisseur du film, l'autodiffusivité de surface sur la facette supérieure du front, l'angle de contact équivalent du film sur le substrat, ainsi que la valeur absolue des énergies de surface se sont révélés être les facteurs qui influencent le plus le taux de rétractation des bords. Dans les modèles isotropes et certains systèmes expérimentaux, des vallées se forment à l'avant des fronts de rétractation et s'approfondissent pour entrer en contact avec le substrat et mener à la rupture du film. Notre modèle suggère que cette forme de rupture ne se produira pas lorsque le front est complètement facetté et que sa surface supérieure est une facette d'équilibre. Pourtant, cette rupture du film peut survenir via l'amincissement de films ainsi que pour des films dont les surfaces supérieures ne forment pas de facettes d'équilibre.

1. Introduction

Except in the rare case of complete wetting, thin films are inherently unstable against capillary forces because their extreme aspect ratios ensure that they are far from their equilibrium shapes. When heated to enable mass transport, capillary forces drive thin films to undergo dewetting, which can occur in the solid state at temperatures well below the melting point. In crystalline materials, the dominant transport mechanism for solid-state dewetting is generally found to be capillary-driven surface diffusion [1–5].

Unwanted dewetting of thin films is often a critical impediment to processing of microelectronic circuits and other micro- and nano-devices and systems [6]. However, dewetting can also be used advantageously to create nanocrystals for memory devices [7], catalysts for carbon nanotube growth [8], catalysts for nanowire growth [9,10] and sensors [11].

The dewetting of single-crystal anisotropic thin films leads to complex structures that are strongly affected by the crystallographic alignment of the film over large areas [4,5,12–14]. When films are patterned via lithography and then dewetted, highly-reproducible complex structures with sub-lithographic feature sizes are produced [15]. However, there is currently no reliable method for quantitatively analyzing the effects of crystalline anisotropy on dewetting, which limits the application of this technique for film patterning.

In this paper, we present a two-dimensional model for shape evolution via capillarity-driven surface diffusion for highly anisotropic dewetting. This model is based on the crystalline method of Carter et al. [16].

2. Dewetting

Dewetting of thin films proceeds at edges, which can exist in the as-deposited film, can be the result of post-deposition film patterning, or can form spontaneously when a film is heated, from the formation of holes by natural processes. As an example of the latter, grain boundary grooves in polycrystalline films can extend through the entire thickness of the film and 'nucleate' holes [17,3]. Once edges are present, they will retract to reduce the surface area. This can, in principle, occur through bulk diffusion processes or by evaporation/condensation processes. However, solid-state dewetting is generally found to proceed by capillary-driven surface diffusion, as described by Mullins [18] and first analyzed in the context of dewetting of films by Brandon and Bradshaw [1] and Srolovitz and Safran [19] for isotropic surface energy and surface diffusivities. An edge with an initially square profile will evolve toward a uniform mean-curvature shape with an equilibrium contact angle with the substrate [19,20]. As dewetting proceeds, a rim develops due to mass accumulation at the moving edge (Fig. 1). The growing rim results in a lower surface curvature, and therefore a lower chemical potential gradient away from the triple line, so the edge retraction rate decreases with time. The retraction distance scales as $t^{2/5}$ [20] in isotropic models.

As a film edge retracts, a valley may form ahead of the moving rim and deepen with time [19–21]. Eventually, the valley touches the substrate, pinching off a line of material, and the cycle begins again with quick adjustment to the equilibrium contact angle, formation of a new rim, and ultimately another pinch-off event [20]. This pinch-off process can repeat to lead to periodic mass shedding [20]. Formation of valleys and pinch-off has been observed in dewetting of single-crystal Ni films [5,22].

Experiments on single-crystal films show that edges with different in-plane crystallographic orientations retract at different rates [23,24]. Anisotropic models for edge retraction must therefore be developed to account for this known experimental phenomenology. Also, facets are commonly observed on the rims of these materials, which must also be accounted for in edge retraction models. Applying Mullins' model to the anisotropic case using a finite-difference method predicts a rim-and-valley film edge profile [21]. However, experiments on single-crystal films do not always show valley formation. For example, valleys are not observed on fully-faceted single-crystal Si films [24,21], Au–Fe films [25], for some Ni film orientations [26]. Therefore, a model for fully-faceted thin films is needed to quantitatively account for anisotropy in retraction rates, and the observations of valleys in some cases and not others.

* Corresponding author.
E-mail address: rzucker@mit.edu (R.V. Zucker).

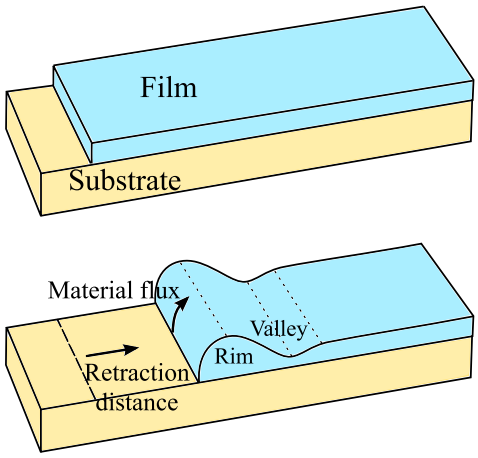

Fig. 1. Isotropic capillary-driven edge retraction. The initially flat film forms the equilibrium contact angle with the substrate, the corner rounds, and the triple line retracts. Mass accumulation at the film edge generates a rim, and a valley follows.

Carter et al. developed a 2D model explicitly for modeling of the evolution of solids with fully-faceted surfaces [16]. Klinger et al. [25] applied this method to modeling of the retraction of thin film edges, and found that no valleys form when a limited number of facet orientations is available, consistent with experimental observations in some systems. However, their implementation does not include topological changes, such as the introduction of new facets.

It should be noted that retracting edges can become unstable and develop fingers [2,24,27,28] or in-plane facets [23]. A 2D model cannot be used to analyze these instabilities. However, when a retracting edge breaks up into in-plane facets, these facets correspond to kinetically stable edges. A quantitative understanding of the retraction of kinetically stable edges can therefore be extended to analyze the motion of such faceted three-dimensional edges [23].

3. Model background

To describe the motion of a two-dimensional surface, an arc length s is used to define position on the surface. The normal vector, $\mathbf{n}(s)$, provides the orientation of the interface. By convention, the normal vector always points outwards, away from the material. Displacements parallel to the local normal vector are tracked as a function of position s and time t. The orientation of the normal vector may in general change with time, but it is defined for any (s,t). The complete evolution of the shape of a material will be obtained by knowing the speed of motion along the surface normal, $v_{\mathbf{n}}$, as a function of time and position.

Mullins developed an expression for $v_{\mathbf{n}}(s,t)$ for isotropic materials [18]. His derivation began with the rate of change of the surface free energy with respect to the volume that has been swept out, $\frac{\mathrm{d}E}{\mathrm{d}V}$, which is equal to the geometric mean curvature, κ, scaled by the surface energy per unit area, γ. The local value of $\frac{\mathrm{d}E}{\mathrm{d}V}$ is related to the local value of the chemical potential: $\frac{\mathrm{d}E}{\mathrm{d}V} = \frac{\mu(s)}{\Omega}$, where Ω is the atomic volume. Because a pure material is being treated here, the chemical potential refers to single species and $\mu(s)$ can be related to the local vapor pressure of the film. When the interface has curvature $\kappa(s) = \frac{\mathrm{d}A}{\mathrm{d}V}$, there is chemical potential difference relative to a flat surface [29]:

$$\Delta\mu(s) = \kappa(s)\gamma\Omega. \tag{1}$$

Therefore, gradients in surface curvature cause gradients in chemical potential, which will drive diffusion of atoms on the surface of the material. The average velocity of surface atoms in response to curvature gradients is given by the Nernst–Einstein relation:

$$\boldsymbol{v}(s,t) = \frac{-D_{\mathrm{s}}}{k_{\mathrm{B}}T}\nabla_{\mathrm{s}}\kappa(s,t), \tag{2}$$

where D_{s} is the surface self-diffusivity and ∇_s is the gradient operator along the surface profile [18]. When the Nernst–Einstein relation is combined with the expression for chemical potential and mass conservation, the velocity is:

$$v_{\mathbf{n}}(s,t) = \frac{D_{\mathrm{s}}\gamma\Omega^2 c}{k_{\mathrm{B}}T}\nabla_{\mathrm{s}}^2\kappa(s,t), \tag{3}$$

where c is the concentration of mobile species on the surface [18]. This governing equation can also be extended to weakly anisotropic materials (i.e., when the surface free energy has continuous derivatives with respect to orientation and all orientations are present on their equilibrium shape [30]). Models based on this analysis typically involve numerical solution of Eq. (3) [19,20,30,21].

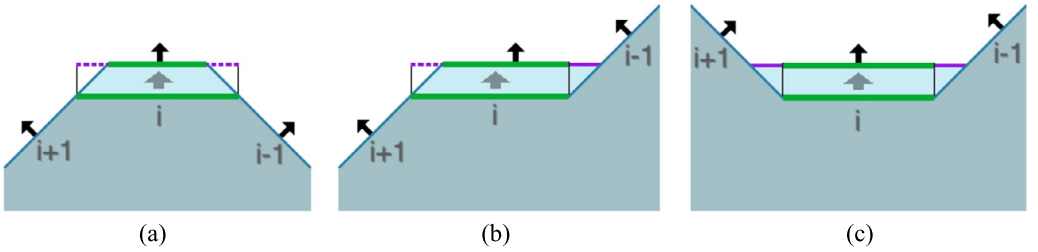

Fig. 2. The change in length caused by moving a facet outwards along its normal, for three types of facet. Facets are labeled in gray, and their normal vectors are drawn in black. (a) A regular facet, which has positive WMC and $\sigma = 1$. Outward motion causes the total length of the facet to decrease. (b) A neutral facet, with zero WMC and $\sigma = 0$. Outward motion causes no net change in the length of the facet. (c) An inverse facet, which has negative WMC and $\sigma = -1$. Outward motion causes the total length of the facet to increase. (Figure after [31].) Color available online.

For fully-faceted bodies, Mullins' formulation is no longer helpful because the facets have zero geometric mean curvature and the corners where facets meet have discontinuous derivatives. Therefore, the chemical potential difference must be written in terms of the more general weighted mean curvature, κ^{γ} (WMC) [31]. The WMC is the change in surface energy with change in volume. In the isotropic limit, WMC reduces to the surface energy times mean curvature, $\gamma\kappa$. For fully-faceted 2D geometries, it can be shown that the WMC of the ith facet on a polygon is [31]:

$$\kappa_i^{\gamma} = \frac{\sigma \Lambda_i}{L_i} \tag{4}$$

where σ_i is 1 if the facet is regular, 0 if the facet is neutral, and -1 if the facet is inverse (see Fig. 2 for explanations of regular, neutral, and inverse), L_i is the length of the facet, and Λ_i is a geometric factor, given by:

$$\Lambda_i = \frac{\gamma_{i+1} - (\mathbf{n}_i \cdot \mathbf{n}_{i+1})\gamma_i}{\sqrt{1 - (\mathbf{n}_i \cdot \mathbf{n}_{i+1})^2}} + \frac{\gamma_{i-1} - (\mathbf{n}_i \cdot \mathbf{n}_{i-1})\gamma_i}{\sqrt{1 - (\mathbf{n}_i \cdot \mathbf{n}_{i-1})^2}}, \tag{5}$$

where $i+1$ indicates the next facet, $i-1$ is the previous facet, and $\mathbf{n}_i$ is the normal vector of the facet [31]. The origin of this expression can be seen from the geometry shown in Fig. 2. This geometric factor is also identical to the length of the facet on the Wulff shape with the same orientation [31]. The Wulff shape is the equilibrium shape of a material with fixed volume when the only contribution to the excess free energy is interfacial energy. It can be found by the Wulff construction [32]. The Wulff construction begins with a plot of $\mathbf{n}\gamma(\mathbf{n})$ for all $\mathbf{n}$ on the unit sphere, where $\mathbf{n}$ is the normal vector to a surface, and $\gamma(\mathbf{n})$ is the excess interfacial energy of that surface. For all orientations, a plane perpendicular to $\mathbf{n}$ is drawn a distance $\gamma(\mathbf{n})$ from the origin. All points on the far side of the plane are discarded. The remaining volume is the equilibrium shape, or Wulff shape. The Wulff shape is always convex, and if composed of flat facets, all facets have $\sigma = 1$. The WMC is uniform on the Wulff shape.

The case of evolution of fully-faceted shapes due to capillarity-driven surface diffusion in two dimensions was treated by Carter et al. [16]. They present the framework for developing the necessary equations, as well as an algorithm to simulate surface diffusion for fully-faceted materials. The model in this work modifies that of [16] to include the effects of the substrate for thin films.

The method begins with the definition of WMC, the definition of chemical potential, and Fick's first law. These are combined with the condition that volume is conserved, and for a moving facet to remain flat, the velocity on that facet must be uniform for all s on that facet. Solving these equations and constraints together gives

$$\mu_i(s) = \mu_i^0 - \frac{J_i}{M_i}s + \frac{v_i}{2M_i}s^2, \tag{6}$$

where s is taken to range from zero to the facet-length L_i on each facet i, μ_i^0 is the chemical potential on facet i at $s = 0$ (units of $\mathrm{J\,m^{-2}}$), J_i is the flux on the facet at $s = 0$ ($\mathrm{m\,s^{-1}}$), M_i is the mobility on the facet times the atomic volume, $M_i = \frac{D_i \Omega}{k_B T}$, where D_i is the diffusivity (yielding units of $\mathrm{m^4\,J^{-1}\,s^{-1}}$), and v_i is the normal velocity of the facet, in units of $\mathrm{s^{-1}}$.

The boundary conditions on facet i are used to find μ_i^0, J_i, and v_i. The flux of atoms leaving the adjacent facet, $i-1$, must equal the flux entering facet i. Similarly, the chemical potential must be smooth and continuous from one facet to the next. For a shape with N facets, these three conditions provide $3N$ equations for $3N$ unknowns, and thus the shape evolution is known, with [16]:

$$v_i = \frac{6M_i(\kappa_i^{\gamma} - \mu_i) + 3J_iL_i}{L_i^2}. \tag{7}$$

The requirements that the mass flux is continuous and the chemical potential is smooth and continuous provide topological constraints on the shape evolution. These constraints are extremely useful for bounding the possible topologies, as discussed below.

For a smooth evolution, the driving force, and therefore the chemical potential, must be finite. This implies that the neighbors of a facet i must have the same orientation as the facet either immediately preceding or following the equivalently-oriented facet on the Wulff shape. If this were not the case, the WMC of intervening facets, with length zero, would be infinite unless $\sigma_i = 0$. If a body were fashioned with a corner that is too sharp, the missing facets would instantaneously appear and blunt the corner. This "neighbor constraint" limits the possible geometries.

During shape evolution, the topology may change due to the formation of new facets or removal of existing facets. The former is referred to as "stepping," while the later is "merging." The formation of a step may be thought of as the accumulation of many atomic ledges. During these topological changes, the chemical potential must change continuously with time. If the chemical potential does not change continuously with time, there is an instantaneous change in the shape morphology, an infinite driving force, and an infinite flux, which is not physically possible. To satisfy continuity, if a new facet is introduced it must initially have zero length. Because the WMC is inversely related to L_i and Λ_i is a positive constant, σ_i must be zero to avoid a singularity. Thus, all new facets must have $\sigma_i = 0$, as in Fig. 2b. Similarly, all facets that disappear must have $\sigma_i = 0$, so their length can go to zero, and the adjacent facets merge.

Another constraint is that steps can only form at places on existing facets where the chemical potential goes through zero. Introducing a zero length facet with zero velocity where the chemical potential is zero has no detectable effect, and the step can then grow to finite length in the next time instant without discontinuous changes in the chemical potential or morphology. The zero velocity constraint is necessary to keep the chemical potential curves smooth and continuous at the point where the facet is introduced.

Finally, steps can only form when

$$\sigma_i \int_0^{L_i} \mu_i(s)\,\mathrm{d}s \geqslant \Lambda_i \tag{8}$$

is satisfied for both pieces of the original facet. If this inequality is not satisfied, the pieces of the original facet will have relative velocities such that they will be driven to merge.

The work by Carter et al., summarized above, provides a complete description of the evolution of fully-faceted bodies via surface diffusion in 2D, which we implement in this work to describe retraction of the edges of thin films.

4. Model implementation

The model developed by Carter et al. was implemented in Wolfram *Mathematica*. The equilibrium shape for the film, the diffusivity on each facet, and the initial film configuration are the inputs. To treat dewetting, the equilibrium shape of the film was taken to be the Winterbottom shape [33], which is essentially the Wulff construction, but incorporating the substrate–film interfacial energy. The surface energy per unit area on the substrate–film interface is $\gamma_{\mathrm{SF}} - \gamma_{\mathrm{SV}}$, where SV refers to the substrate–vapor interface and SF refers to the substrate–film interface. This is the relevant quantity because for every unit of SF interface removed during dewetting, a unit of SV is created.

To iterate through time, the chemical potential on each facet is computed using Eqs. (6) and (7) and a step is introduced at all points where the chemical potential is zero. The "sense" of the step (whether its normal is that of the preceding facet or the following facet on the equilibrium shape) is opposite the derivative of the chemical potential at the zero point [16]. To ensure that the step is allowed, Eq. (8) is computed for each half of the host facet. The step is kept only if the inequality is satisfied for both halves. Additionally, any steps on the film–substrate interface are discarded.

The surviving steps are checked again, this time for stability with respect to time. If the equality in Eq. (8) is exactly satisfied, the relative velocities of the two halves are zero. Only steps which will grow in length are kept; steps which would shrink and disappear in the subsequent time step are discarded. This leaves only the steps which are stable. The exact moment when a step becomes favorable usually falls between numerical time steps, so the appropriate placement of each step must be found using a binary search to choose the position that will make its initial velocity zero.

The stable steps are incorporated into the shape, and the chemical potential, velocity, and flux are recalculated for each facet. If the velocities of adjacent facets will cause them to become coplanar, then the intervening facet must reach zero length and the adjacent facets will merge. This is tested two ways: either the two adjacent facets are separated by a very small distance and have velocities such that they will become coplanar, or the two adjacent facets actually "overshoot" being coplanar, which would cause the intervening facet to change "sense." In either case, a merge occurs.

Finally, the shape is checked for major topological changes, which causes the outward normal of the intervening facet to reverse direction. If two corners or edges, which are not adjacent along the s coordinate, are touching (or within a few atomic radii of each other), the film is split into two or more disconnected parts. This occurs, for example, during pinch-off due to film thinning.

With stepping, merging, and breaking complete, the chemical potential, velocity, and flux are again recalculated for each facet. The time step $\mathrm{d}t$ is set by the Courant–Friedrichs–Lewy (CFL) condition, i.e., $\mathrm{d}t$ cannot exceed $1/v_{\max}$, where $v_{\max}$ is the speed of the fastest-moving facet on the shape at the current time, in units of s^{-1}. This choice of time step ensures that the evolution conserves volume and is stable. Each facet is then moved along its normal by an amount $v_i a_0\,\mathrm{d}t$, where a_0 is the atomic size, and the whole process is repeated.

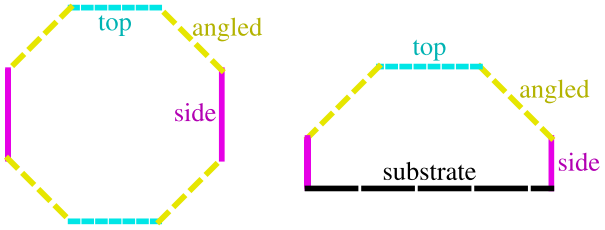

Fig. 3. Reference equilibrium shapes. Left: the Wulff shape is assumed to be octagonal. There are three crystallographically-distinct facets present: the side facet, the angled facet, and the top facet. Right: the Winterbottom shape for the film. The Wulff shape of the film material is truncated through its inversion center to achieve an equivalent wetting angle of 90°. Color available online.

In practice, stepping, merging, and breaking are quite rare. Stepping usually occurs in the first time step because the film is far from equilibrium, and the creation of new facets is necessary to accommodate the tremendous flux of material from the film edges onto the top of the film. Merging typically occurs near the end of the evolution, as the two ends of the retracting film meet. Breaking may or may not occur, and depends on a variety of factors, including relative diffusivity values for different facets and the initial aspect ratio of the film, discussed in more detail below.

5. Reference film

Edge retraction is discussed below for a reference film with an octagonal Wulff shape (Fig. 3). This shape is chosen because FCC and BCC materials usually have Wulff shapes which are octagonal in cross-section, i.e., shapes composed of (100), (111), and (110)-type facets. The equivalent contact angle of the film on the substrate is taken to be 90°, resulting in an equilibrium shape equivalent to the Wulff shape truncated at its center (Fig. 3) [33]. The reference diffusivity is taken to be that of Ni at 900 °C on the (100) facet, $D_0 = 5.53 \times 10^{-11}$ m^2 s^{-1} [34]. This value was chosen because it falls roughly in the middle of the range observed for FCC materials [35]. The diffusivity of the substrate–film interface was taken to be $10^{-5} D_0$ because interfacial diffusivities are usually several orders of magnitude smaller than surface diffusivities, and the model is insensitive to this value as long as it is less than $\sim 10^{-2} D_0$. The reference surface energy is taken to be 2.0 J m^{-2}. This was chosen because solid–vapor interfaces for metals typically have surface energies on the order of 0.4–4 J m^{-2} [36], and 2 J m^{-2} falls in the middle of this range. The reference film shape is 100 μm wide and 100 nm thick. This size was chosen for comparisons with the experiments of Kim et al. [26]. The reference annealing time is 24 h.

6. Results and discussion

6.1. Reference film retraction

The evolution of a fully-faceted thin film begins with a change in topology. At $t = 0$, a step is introduced on the top facet ~ 200 nm from each of the film edges. This step initiates the formation of a rim. Subsequently, the rim expands both in height and width as the edges retract (Figs. 4, 5). The bulk of the film thins linearly with time as material is driven towards to rims. The thinning has a slope of -1.24×10^{-4} h^{-1}, where the current height is normalized to the initial height. The formation of a valley is not thermodynamically favorable.

6.2. Numerical sensitivity

The evolution is initially fast and slows with time. Therefore, the model has a tendency to slightly overestimate the retraction distance, due to the discretization in time. However, if the CFL condition is satisfied, this overestimation is generally less than a percent, and has first order convergence as the time step is decreased.

6.3. The influence of film parameters on the rate of retraction

6.3.1. Diffusivity anisotropy

Diffusivities were varied for the facets present on the reference film to investigate the influence of diffusivity anisotropy on edge retraction, as shown in Fig. 6. The results were fit to $x_o = ct^n$, where x_o is the retraction distance, t is time, and c and n are constants.

Changes in the diffusivities have strong effects on the absolute magnitudes of the retraction distances (c), but have relatively weak effects on the scaling exponent n. Using the nomenclature in Fig. 3, the diffusivity on the top facet has the biggest impact on c, the diffusivity of the angled facet has roughly half the effect of the top facet, and the diffusivity on the side facet is inconsequential. If the diffusivities on the top and side facets are adjusted together, such as in the case of 4-fold symmetry, the retraction distance is not significantly different from the case in which the diffusivity on only the top facet is adjusted.

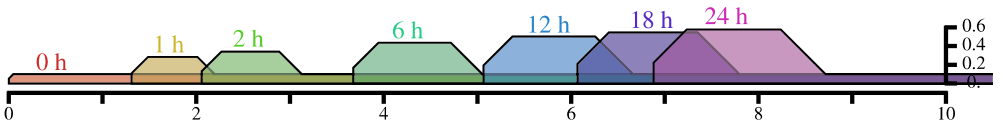

Fig. 4. The reference film edge profile is shown for various times after the annealing begins. The aspect ratio is 1:1, and the units of both the vertical and horizontal scale are micrometers. Color available online.

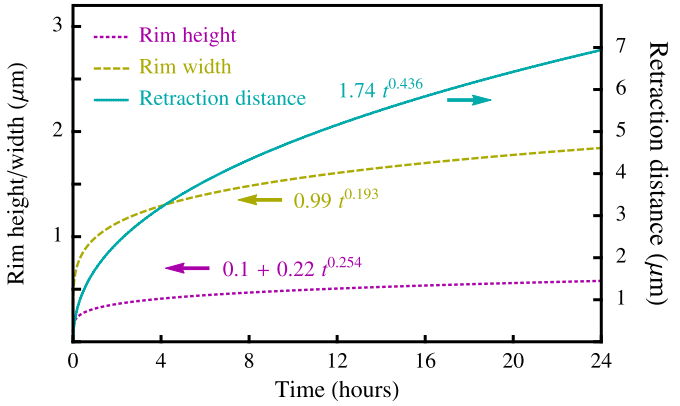

Fig. 5. The retraction distance, the rim height, and the rim width for the reference film as a function of time. The ct^n fit is shown adjacent to each curve. The rim height fit has the constant included because the rim height at $t = 0$ is 0.1 μm. Color available online.

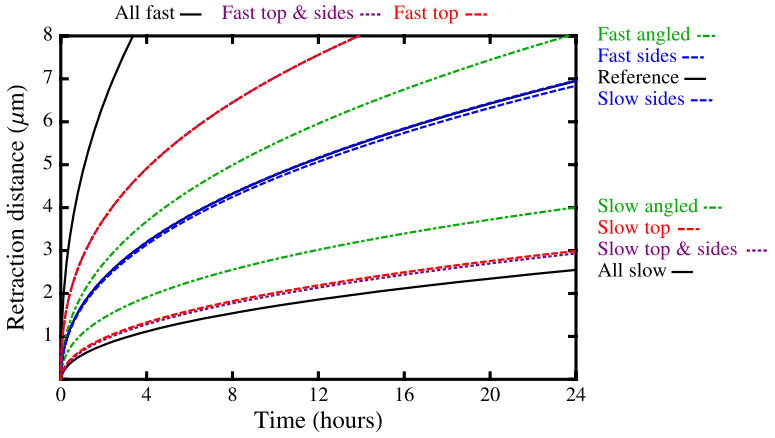

Fig. 6. The diffusivity on each set of symmetrically-related facets was changed to show its effects on the retraction distance vs. time. The ct^n fit parameters for each curve are listed in Table 1. Color available online.

Table 1
The diffusivity on each facet and fit parameters for each curve shown in Fig. 6 are listed.

Curve label	D_{top}/D_0	D_{angled}/D_0	D_{side}/D_0	c	n
Reference	1	1	1	1.740	0.436
All fast	10	10	10	4.795	0.419
All slow	0.1	0.1	0.1	0.585	0.464
Fast top	10	1	1	2.835	0.394
Slow top	0.1	1	1	0.701	0.457
Fast angled	1	10	1	1.996	0.440
Slow angled	1	0.1	1	1.076	0.414
Fast sides	1	1	10	1.745	0.436
Slow sides	1	1	0.1	1.705	0.438
Fast top & sides	10	1	10	2.838	0.394
Slow top & sides	0.1	1	0.1	0.672	0.465

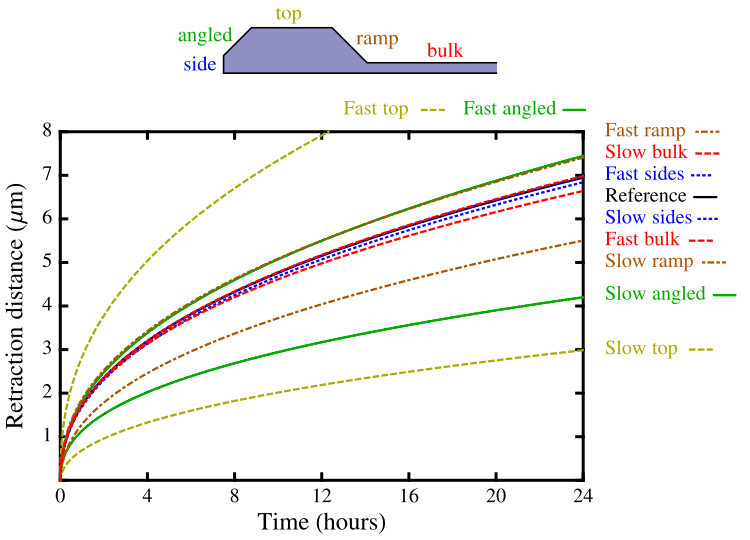

Fig. 7. The effect of changes in the diffusivity on individual facets on the retraction distance vs. time. The labeling convention is shown in the schematic above the plot. "Slow" corresponds to a diffusivity of $0.1D_0$ on the facet of interest and $1D_0$ on all other facets, while "fast" corresponds to $10D_0$ on the facet of interest. The fit parameters to each curve are tabulated in Table 2. Color available online.

Table 2
The diffusivity on each facet and the ct^n fit parameters for each curve shown in Fig. 7 are listed.

Curve label	D_{side}/D_0	D_{angled}/D_0	D_{top}/D_0	D_{ramp}/D_0	D_{bulk}/D_0	c	n
Reference	1	1	1	1	1	1.740	0.436
Fast sides	10	1	1	1	1	1.745	0.436
Slow sides	0.1	1	1	1	1	1.705	0.438
Fast angled	1	10	1	1	1	1.826	0.443
Slow angled	1	0.1	1	1	1	1.144	0.410
Fast top	1	1	10	1	1	2.838	0.412
Slow top	1	1	0.1	1	1	0.701	0.457
Fast ramp	1	1	1	10	1	1.877	0.432
Slow ramp	1	1	1	0.1	1	1.309	0.453
Fast bulk	1	1	1	1	10	1.740	0.422
Slow bulk	1	1	1	1	0.1	1.740	0.438

To identify which individual facet has the greatest effect on the retraction rate, the symmetry was broken, and the diffusivity of each facet was adjusted independently. The results are shown in Fig. 7. The diffusivity on the facet at the top of the rim has the largest influence, followed by the ramp, angled, side, and bulk facets. This ordering can be understood by considering the relationship between the chemical potential and the mass flux, as shown in Fig. 8. The chemical potential profile evolves to the shape of the one shown in this figure within a few minutes of the start of retraction, and gradually decreases in peak magnitude with time. The diffusivity on the facet which must accommodate the highest flux will set the retraction rate. The larger the chemical potential gradient, the higher the flux, and therefore the more sensitive the retraction rate is to the diffusivity on that facet.

The diffusivity on the bulk facet has almost no effect on the retraction rate, despite being orders of magnitude larger than the other facets. However, its effects are reversed from the rest of the facets. Slowing the bulk facet diffusivity accelerates retraction because the flux of material from that facet is towards the rims. Feeding the rim with material from the bulk offsets diffusion from the triple line.

6.3.2. *Value of surface energies*

The relative values of surface energy of each facet must fall within a narrow range of each other because the Wulff construction excludes orientations with significantly different energies. For the octagonal Wulff shape explored here with $\gamma_{side} = \gamma_{top}$, both facets appear only if $\frac{1}{\sqrt{2}} \sim 0.707 < \frac{\gamma_{angled}}{\gamma_{top}} < \sqrt{2} \sim 1.414$. As a result, changing the relative surface energies has a relatively weak effect on the retraction distance. The retraction distance for $\frac{\gamma_{angled}}{\gamma_{top}} = 1.3$ is about 1.24 times that for $\frac{\gamma_{angled}}{\gamma_{top}} = 0.8$. The exponent is even more weakly affected by surface energy changes in this range, $n = 0.442$ for $\frac{\gamma_{angled}}{\gamma_{top}} = 1.3$ and $n = 0.426$ for $\frac{\gamma_{angled}}{\gamma_{top}} = 0.8$.

The effect of relative surface energy is secondary to the effect of differences in diffusivity. Changing the relative surface energy changes the length of each facet exposed during the retraction, allowing the longer facet's diffusivity to have a stronger effect.

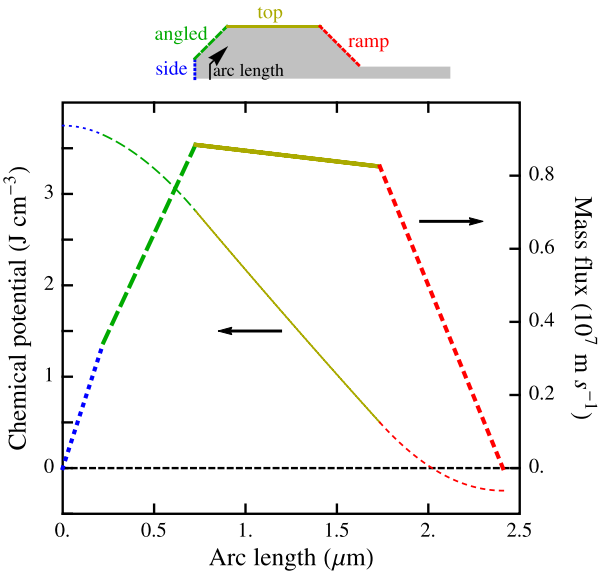

Fig. 8. The chemical potential and mass flux as a function of the arc length at $t = 24$ h. The curves are divided into four segments corresponding to the four facets shown in the small figure above the plot. Chemical potential is set to be zero on an infinitely long facet. The chemical potential varies parabolically on each facet with curvature proportional to the normal velocity of the facet. The mass flux is proportional to the derivative of the chemical potential with respect to arc length. The curves for the bulk facet and substrate interface are not shown because they are orders of magnitude larger in length and have fluxes that are several orders of magnitude smaller than the four facets shown. These data are for the reference film. Color available online.

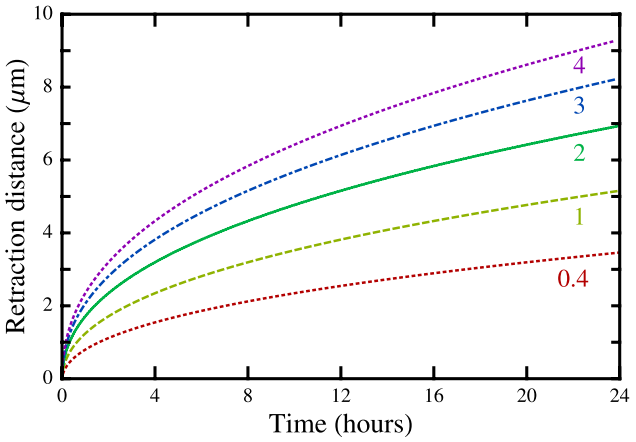

Fig. 9. The influence of the absolute value of surface energy on the film edge retraction distance vs. time. Each curve is labeled with the surface energy in $\mathrm{J\,m^{-2}}$. The ct^n fit to each curve is shown in Table 3. Color available online.

Table 3
The ct^n fit parameters for each curve in Fig. 9 are listed.

Curve label	c	n
0.4 $\mathrm{J\,m^{-2}}$	0.794	0.468
1 $\mathrm{J\,m^{-2}}$	1.231	0.455
Reference, 2 $\mathrm{J\,m^{-2}}$	1.697	0.447
3 $\mathrm{J\,m^{-2}}$	2.041	0.443
4 $\mathrm{J\,m^{-2}}$	2.323	0.440

While the relative values of the surface energies have a weak effect on the retraction rate, the absolute values of the surface energies have a stronger effect. However, in nature, surface energies generally fall in the range ~ 0.5 $\mathrm{J\,m^{-2}}$ to 4 $\mathrm{J\,m^{-2}}$. The effects of changing γ_0 over this range are shown in Fig. 9. Again, the exponent is only very weakly affected.

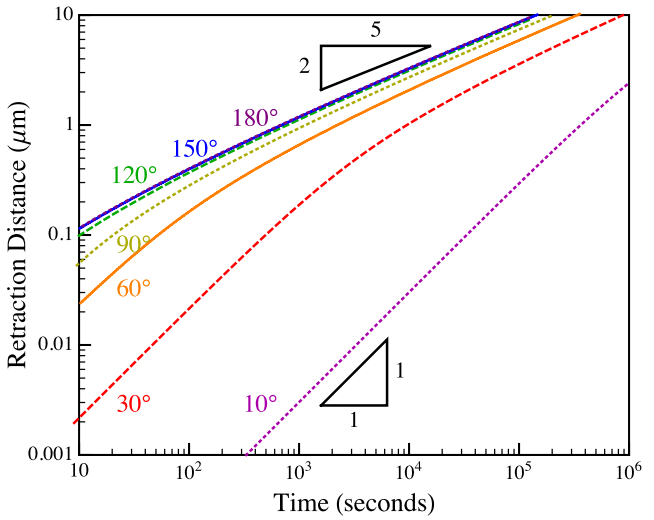

Fig. 10. The effect of changing the $\gamma_{SV} - \gamma_{SF}$ on the retraction distance vs. time. Each curve is labeled with the equivalent contact angle, $\cos^{-1}(\frac{\gamma_{SV}-\gamma_{SF}}{\gamma_{FV}})$. Color available online.

6.3.3. *Effective wetting angle:* $\cos^{-1}(\frac{\gamma_{SV}-\gamma_{SF}}{\gamma_{FV}})$

The retraction rate is extremely sensitive to $\gamma_{SV} - \gamma_{SF}$, where γ_{SV} is the surface energy of the substrate in contact with vapor and γ_{SF} is the substrate–film interfacial energy. Although the physical contact angle between the film and the substrate is highly constrained by the anisotropy, an equivalent to the isotropic contact angle can be defined as $\cos^{-1}(\frac{\gamma_{SV}-\gamma_{SF}}{\gamma_{FV}})$, where γ_{FV} is the surface energy of the top facet on the film. Fig. 10 shows the results of systematically varying $\gamma_{SV} - \gamma_{SF}$. The film retraction accelerates for higher equivalent contact angles, and approaches zero as the equivalent contact angle goes to zero. The power law exponent is 1 in the limit of complete wetting and at short times, and approaches 2/5 at long times. These trends are in excellent agreement with the isotropic model [20]. Retraction is initially linear because the rim has not yet had sufficient time to build in height, so the WMC of the film edge is essentially unchanged, and the driving force to retract is constant.

For contact angles less than 65.5°, the Winterbottom shape is trapezoidal, and the side facets are absent. Similarly, for contact angles greater than 114.5°, the Winterbottom shape has eight sides and includes the angled facets below the sides. However, the abrupt transition in topology as the contact angle changes does not cause an abrupt change in the retraction rate. This is because the influence of each facet is proportional to the length of that facet on the Winterbottom shape, so the transition is smooth.

6.3.4. *Film thickness*

If the width of the film is fixed and the thickness is varied, a strong effect on the retraction rate is observed (Fig. 11). The total retraction distance per unit time scales as $h^{-1/2}$, where h is the film thickness. The exponent is slightly time-dependent, being -0.520 at $t = 1$ h and -0.483 at $t = 24$ h. For the thinnest film, the exponent in the ct^n fit is 0.382 for the 10-nm-thick film immediately before it undergoes pinch-off by film thinning after 56 h of retraction. This indicates that 2/5 is not the minimum value the exponent may have.

6.3.5. *Film width*

The retraction rate is largely insensitive to the initial width of the film. However, the exponent and retraction rate do increase slightly as the film width increases. The retraction distance of a 25-μm-wide film is only about 8.8% less than that of an 800-μm-wide film. The exponent is 0.418 for the 25-μm-wide film, and 0.443 for the 800-μm-wide film. The width dependence is due to the small flux of material from the bulk into the rims. If the diffusivity of the bulk facet is set to $10^{-5}D_0$, there is no width dependence. This follows because the two retracting edges are independent until they impinge. The case of zero diffusivity on the bulk facet represents the "infinitely wide" film. The ct^n power law fit for 24 h of retraction is $c = 1.742$ and $n = 0.438$. For 250–1000 h of retraction, the power law fit is $c = 1.903$ and $n = 0.415$.

6.3.6. *Facet orientation*

The orientation of the normal to the angled facet (Fig. 3) can be changed to represent different crystallographic orientations. The reference film has a 45° normal, as would be the case for a cubic crystal with (001) as the top facet, (110) as the angled facet, and (100) as the side facet. As an example of another common orientation, if the normal is 62.6° above the horizontal, this could represent a slice through a cubic material with (011) as the top facet, (111) as the angled facet, and (100) as the side facet. The model was found to be completely insensitive to the orientation of the angled facet. The exponent in the power law fit was changed by less than 0.1% by changing the orientation. The retraction distance was changed by

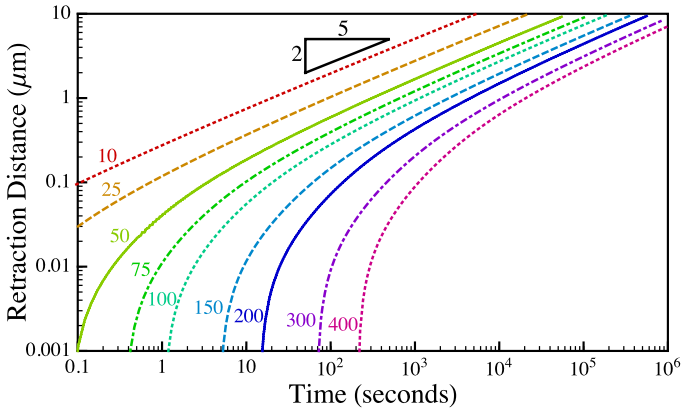

Fig. 11. The effect of changing the thickness of the film on the retraction distance as a function of time. Each curve is labeled with the thickness of the film, in nanometers. Color available online.

less than 1%. This follows because the model is essentially one-dimensional, tracking properties along the surface coordinate only.

6.3.7. Film edge geometry

The model is insensitive to the initial geometry of the film edge. A nearly rectangular film edge was constructed, having an angled facet which is 4 nm in length and a side facet 96 nm long, and was compared to a nearly trapezoidal film edge, having an angled facet which was 133 nm long and a side facet 6 nm long. After 24 h of retraction the retraction distance differed by less than 0.4% due to changes in the film edge profile. This is because the film edge reaches the shape shown in Fig. 4 very quickly, within about 5 min, so it has little time to influence the retraction rate.

6.3.8. Number of facets

The model is insensitive to the number of facets present on the equilibrium shape. The retraction distance of materials with square, hexagonal, and 16-gonal Wulff shapes was found to vary by less than 4% from the retraction distance of a film with the octagonal reference Wulff shape after 24 h. The exponent of retraction is unchanged. The only systematic differences are that the bulk of the film thins faster and the rim is taller when more facets are present. This implies that in the limit of infinite facets, i.e. isotropy, the bulk film would be driven to thin at a high rate and one might expect a valley to form as diffusion can no longer supply material fast enough to achieve uniform thinning.

6.4. Comparison with experiments

The properties of Ni at 890 °C were input into this model and compared with experimental results for the retraction of 130-nm-thick Ni films on MgO for four crystallographically-distinct orientations. The results of this study are discussed at length in Kim et al., summarized in Fig. 3 of that reference [26]. Both experiments and the model showed retraction distances varying by nearly a factor of 2, depending on the edge orientation. The model matched experimental results to within 10% for a (001) film with an edge retracting in the [100] direction, and a (011) film with an edge retracting in the [100] direction. The model over-estimated the retraction distance for a (001) film retracting in the [110] direction by nearly a factor of 2, and underestimated the retraction of a (011) film retracting in the $[1\bar{1}0]$ direction by about 50%. The discrepancy between the model and experiment can be accounted for by error in the reported values of diffusivities for Ni on the facets present, and the uncertainty in the interfacial energy between Ni and the MgO substrate.

6.5. Pinch-off

This model predicts that valleys do not form ahead of the retracting rim with a flat top surface, which is distinct from isotropic and non-fully faceted anisotropic models [20,21]. Experiments indicate that for fully-faceted films, valleys are absent, in agreement with this model [21,24–26]. Even if valleys are artificially introduced in the model at $t = 0$, they quickly fill in and disappear because they are not stable morphologies. However, the bulk film is thinning, and if the aspect ratio of the film is sufficiently high, the film can thin to zero thickness before the retracting edges meet (Fig. 12a). For a 100-μm-wide film, pinch-off by film thinning takes a few hundred hours. The thickness for which pinch-off occurs by film thinning in a 100-μm-wide film is between 30 and 40 nm. For thicker films, the rims interact before pinch-off occurs (Fig. 12b) and the thickness at the center begins to go up (Fig. 13). In this case, the rims merge.

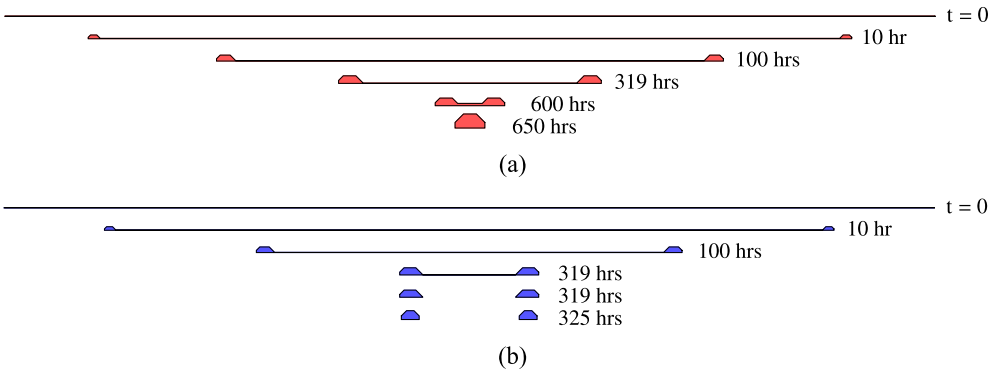

Fig. 12. Profiles of (a) 40-nm-thick and (b) 30-nm-thick 100-μm-wide film dewetting until equilibrium is reached. The 40-nm-thick film thins during dewetting, but the rims interact before pinch-off is achieved. The 30-nm-thick film thins until the bulk of the film has zero thickness. The time shown is the number of hours after the initiation of dewetting.

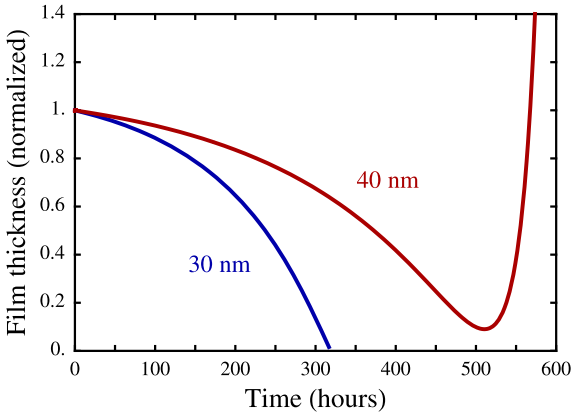

Fig. 13. The bulk film height normalized to the initial film thickness as a function of time is shown for a 100-μm-wide film. The 30-nm-thick film undergoes pinch-off after 319 h, and leaves two lines of material. The 40-nm-thick film initially thins, but as the two rims approach the center, they begin to interact and cause thickening, ultimately merging and leaving a single line of material. The final height of the 40-nm-thick film is 38.6 times its original height.

6.6. Valley formation

A valley can be produced with this model if there is no equilibrium facet parallel to the substrate, so that the top of the film instead has a sawtooth morphology (Fig. 14). Such geometry could be generated if the top surface of a thin film underwent a faceting instability. A faceting instability occurs when a flat physical surface does not correspond to an equilibrium facet (a facet on the Wulff shape). In this case, the originally flat surface will evolve to become non-planar, and be composed of alternating equilibrium facets [37,38].

If the top of the film has a sawtooth morphology, then as the edge retracts, a valley develops (Fig. 14). The film is initially 100 nm thick on average, and is identical to the reference film, except that the octagonal Wulff shape was rotated by 22.5° so that a vertex, not a facet, is at the top of the film. Pinch-off by valley formation is achieved after 57.3 minutes. The final morphology and time to pinch-off is insensitive to the length scale of the sawtooth pattern of facets. The retraction rate up until pinch-off is very similar to that of the reference film. The film profile shows not only a rim and a valley, but also a secondary, smaller rim and valley. This is similar to the isotropic case, which leads to a decaying undulatory profile, as also seen in the isotropic model [20].

7. Summary and conclusions

A two-dimensional model for the capillarity-driven evolution of bodies with fully-faceted shapes developed by Carter et al. [16] was adapted to modeling of solid-state dewetting of fully-faceted thin films. Capillarity-induced retraction of an edge of a thin film was studied in detail, and the effects of adjusting various physical parameters on the retraction rate were explored.

The major factors which determine the retraction rate of a thin film, according to this model, are: the film thickness, the atomic diffusivity on the top facet and the angled facet, the equivalent contact angle of the film on the substrate, and the absolute value of the surface energy. The edge retraction distance scales with the film thickness h as $h^{1/2}$.

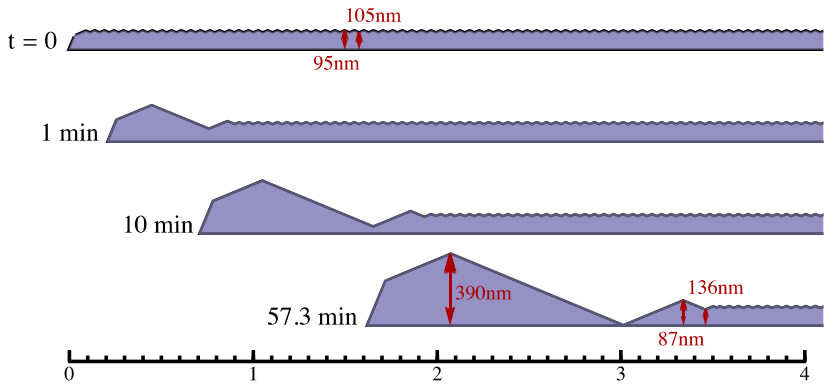

Fig. 14. The retraction of a film with a sawtooth morphology on the top surface. The scale bar at the bottom is in micrometers.

If all of the material removed from the edge of the film accumulated in the rim, edge retraction should proceed as $t^{2/5}$ [1]. However, there is a flux of material to the rim from the bulk, which slowly decreases the exponent in the power law fit. The same is true of isotropic films; they do not obey a power law because of additional material supplied by the deepening valley. Therefore, there is no time-independent value of the power law fit exponent n for either isotropic or anisotropic films.

When applied to a real system, this model shows good agreement with experimental edge retraction results for the Ni on MgO system, discussed at length by Kim et al. [26]. In this case, the retraction distance scales with time as ct^n, where c is a constant and $n \sim 2/5$. The increase in the thickness of the rim and the rim width scale with $n \sim 1/5$. These scaling parameters are not strongly affected by reasonable variations in facet surface energies or the atomic diffusivities on the facets. However, the proportionality constant c is strongly affected by the diffusivities, especially on the top facet. The energy per area of the film–substrate interface, which affects the equivalent contact angle, can strongly affect n.

In isotropic models, valleys form ahead of retracting rims and can eventually lead to pinch-off. In experimental studies of single-crystal films, valleys are often absent at retracting edges. The model presented here predicts that pinch-off does not occur through valley formation in fully-faceted films when the top facet is an equilibrium facet. However, if a non-equilibrium top facet decomposes due to a faceting instability, valleys do form ahead of the rim and can lead to pinch-off. Otherwise, the only mechanism for pinch-off is a uniform film thinning of the film ahead of the rim.

Acknowledgements

The authors gratefully acknowledge Victor Brunini for his contributions to the development of the code for this model. This work was partially supported by the Singapore-MIT Alliance and NSF grant number DMR-1104610. R.Z. was partially supported by the National Science Foundation under Grant No. 1122374.

References

[1] R. Brandon, F.J. Bradshaw, The mobility of the surface atoms of copper and silver evaporated deposits, Royal Aircraft Establishment Technical Report 66095, March 1966.
[2] E. Jiran, C.V. Thompson, Capillary instabilities in thin films, J. Electron. Mater. 19 (1990) 1153.
[3] E. Jiran, C.V. Thompson, Capillary instabilities in thin, continuous films, Thin Solid Films 208 (1992) 23.
[4] D. Danielson, D. Sparacin, M. Jurgen, L. Kimerling, Surface-energy-driven dewetting theory of silicon-on-insulator agglomeration, J. Appl. Phys. 100 (2006) 083507.
[5] J. Ye, C.V. Thompson, Mechanisms of complex morphological evolution during solid-state dewetting of single-crystal nickel thin films, Appl. Phys. Lett. 97 (2010) 071904.
[6] C. Jahan, O. Faynot, L. Tosti, J.M. Hartmann, Agglomeration control during the selective epitaxial growth of Si raised sources and drains on ultra-thin silicon-on-insulator substrates, J. Cryst. Growth 280 (2005) 530.
[7] S. Rath, M. Heilig, H. Port, J. Wrachtrup, Periodic organic nanodot patterns for optical memory, Nano Lett. 7 (2007) 3845.
[8] M. Chhowalla, K.B.K. Teo, C. Ducati, N.L. Rupesinghe, G.A.J. Amaratunga, A.C. Ferrari, D. Roy, J. Robertson, W.I. Mine, Growth process conditions of vertically aligned carbon nanotubes using plasma enhanced chemical vapor deposition, J. Appl. Phys. 90 (2001) 5308.
[9] V. Schmidt, J.V. Wittemann, S. Senz, U. Gosele, Silicon nanowires: A review on aspects of their growth and their electrical properties, Adv. Mater. 21 (2009) 2681.
[10] A. Colli, A. Fasoli, P. Beecher, P. Servati, S. Pisana, Y. Fu, A. Flewitt, W. Mine, J. Robertson, C. Ducati, S. De Franceschi, S. Hofmann, A. Ferrari, Thermal and chemical vapor deposition of Si nanowires: Shape control, dispersion and electrical properties, J. Appl. Phys. 102 (2007) 034302.
[11] J. Mizsei, Activating technology of SnO_2 layers by metal particles from ultra thin metal films, Sens. Actuators B, Chem. (1993) 328.
[12] R. Nuryadi, Y. Ishikawa, M. Tabe, Formation and ordering of self-assembled Si islands by ultrahigh vacuum annealing of ultrathin bonded silicon-on-insulator structure, Appl. Surf. Sci. 159 (2000) 121.
[13] P. Sutter, W. Ernst, Y.S. Choi, E. Sutter, Mechanisms of thermally induced dewetting of ultrathin silicon-on-insulator, Appl. Phys. Lett. 88 (2006) 141924.
[14] Y. Fan, R. Nuryadi, Z. Burhanudin, M. Tabe, Thermal agglomeration of ultrathin silicon-on-insulator layers: Crystalline orientation dependence, Jpn. J. Appl. Phys. 47 (2008) 1461.
[15] J. Ye, C.V. Thompson, Templated solid-state dewetting to controllably produce complex patterns, Adv. Mater. 23 (2011) 1567.

[16] W.C. Carter, A.R. Roosen, J.W. Cahn, J.E. Taylor, Shape evolution by surface attachment limited kinetics on completely faceted surfaces, Acta Metall. Mater. 43 (1995) 4309.
[17] D.J. Srolovitz, S.A. Safran, Capillary instabilities in thin films. I. Energetics, J. Appl. Phys. 60 (1986) 247.
[18] W.W. Mullins, Theory of thermal grooving, J. Appl. Phys. 28 (1957) 333.
[19] D.J. Srolovitz, S.A. Safran, Capillary instabilities in thin films. II. Kinetics, J. Appl. Phys. 60 (1986) 255.
[20] H. Wong, P.W. Voorhees, M.J. Miksis, S.H. Davis, Periodic mass shedding of a retracting solid film step, Acta Mater. 48 (2000) 1719.
[21] E. Dornel, J.-C. Barbé, F. de Crécy, G. Lacolle, J. Eymery, Surface diffusion dewetting of thin solid films: Numerical method and application to Si/SiO_2, Phys. Rev. B 73 (2006) 115427.
[22] J. Ye, C.V. Thompson, Regular pattern formation through the retraction and pinch-off of edges during solid-state dewetting of patterned single crystal films, Phys. Rev. B 82 (2010) 193408.
[23] J. Ye, C.V. Thompson, Anisotropic edge retraction and hole growth during solid-state dewetting of single crystal nickel thin films, Acta Mater. 59 (2011) 582.
[24] E. Bussmann, F. Cheynis, F. Leroy, P. Muller, O. Pierre-Louis, Dynamics of solid thin-film dewetting in the silicon-on-insulator system, New J. Phys. 13 (2011) 043017.
[25] L. Klinger, D. Amram, E. Rabkin, Kinetics of a retracting solid film edge: The case of high surface anisotropy, Scr. Mater. 64 (2011) 962.
[26] G.H. Kim, R.V. Zucker, J. Ye, W.C. Carter, C.V. Thompson, Quantitative analysis of anisotropic edge retraction by solid-state dewetting of thin single crystal films, J. Appl. Phys. (2013), in press.
[27] F. Leroy, F. Cheynis, T. Passanante, P. Mueller, Dynamics, anisotropy, and stability of silicon-on-insulator dewetting fronts, Phys. Rev. B 85 (2012) 195414.
[28] W. Kan, H. Wong, Fingering instability of retracting solid film edge, J. Appl. Phys. 97 (2005) 043515.
[29] C. Herring, W.E. Kingston (Eds.), The Physics of Powder Metallurgy, McGraw–Hill, New York, 1951, p. 143.
[30] W. Zhang, I. Gladwell, Evolution of two-dimensional crystal morphologies by surface diffusion with anisotropic surface free energies, Comput. Mater. Sci. 27 (2003) 461.
[31] J.E. Taylor, Mean curvature and weighted mean curvature, Acta Metall. Mater. 40 (1992) 1475.
[32] G. Wulff, Zur Frage der Geschwindigkeit des Wachstums und der Auflösung der Kristallflächen, Z. Kristallogr. 34 (1901) 449.
[33] W.L. Winterbottom, Equilibrium shape of a small particle in contact with a foreign substrate, Acta Metall. 15 (1967) 303.
[34] P.S. Maiya, J.M. Blakely, Surface self-diffusion and surface energy of nickel, J. Appl. Phys. 38 (1967) 698.
[35] P.M. Agrawal, B.M. Rice, D.L. Thompson, Predicting trends in rate parameters for self-diffusion of FCC metal surfaces, Surf. Sci. 515 (2002) 21.
[36] L. Vitos, A.V. Ruban, H.L. Skriver, J. Kollar, The surface energy of metals, Surf. Sci. 411 (1998) 186.
[37] S. Seo, C. Euaruksakui, D.E. Savage, M.G. Lagally, P.G. Evans, Nanostructure formation in the initial roughening of a thin silicon sheet, Phys. Rev. B 81 (2010), 041302(R).
[38] F. Buatier de Mongeot, W. Zhu, A. Molle, R. Buzio, C. Boragno, U. Valbusa, E.G. Wang, Z. Zhang, Nanocrystal formation and faceting instability in A1(110) homoepitaxy: True upward adatom diffusion at step edges and island corner, Phys. Rev. Lett. 91 (2003) 016102.